Uncovering the role of superplasticizer in developing nano-engineered ultra-high-performance concrete

Lili Wang, Yitong Ma* and Liangwei Li

School of Materials Science and Engineering, Wuhan University of Technology, Wuhan, China

The effect of superplasticizer (SP) on the performance of ultra-high-performance concrete (UHPC) and ultra-high-performance fiber-reinforced concrete (UHPFRC) has been systematically investigated aiming to optimize the use of SP. The slump flow, and V-funnel time were employed to evaluate the impact of SP on the workability, while compressive strength had been used for mechanical property. Moreover, the packing density, as well as the water film thickness had been calculated to uncover the mechanism. The obtained results indicated that the addition of SP improved the workability of specimens with an ultimate-low water-to-binder (W/B) ratio, while it benefited the strength development of UHPC with a lower W/B ratio. This novel phenomenon (SP enhances the mechanical properties of UHPC) is due to the fact that SP reduced the water film thickness and enhanced the packing structure, therefore resulting in an increased compressive strength. For UHPFRC, similar trends can be witnessed regarding the flowability. However, the alternation of the fresh behavior of UHPFRC, attributed to the inclusion of SP, had an obvious impact on the fiber distribution, which altered the strength development of UHPFRC. This study revealed the significant effect of SP on the performance, especially on the strength development, of UHPC and UHPFRC.

KEYWORDS

superplasticizer, ultra-high performance concrete, ultra-high performance fiber-reinforced concrete, packing system, fiber distribution

1 Introduction

Superplasticizer (SP) remains an essential component of modern concrete since it brings about multiple advantages to the building industry (Boscaro et al., 2021). Due to its effective water reduction effect, which is attributed to both an enhanced steric hindrance effect and a charge neutralization effect (as shown in Figure 1), SP can disperse the accumulated particles and release the locked water (Othmane et al., 2012). Consequently, the inclusion of SP results in either an improved workability by increasing the amount of excess water or a higher strength by decreasing the water-to-binder (W/B) ratio while maintaining the same flowability requirement (Lange et al., 2014).

The influence of SP on the performance of concrete has been systematically investigated (Zhang et al., 2019; Ma et al., 2020; Zhu et al., 2021; Ammar, 2011; Zhang and Kong, 2015; He et al., 2021; Zhang and Kong, 2014; Zeyad and Almalki, 2020; Nakul et al., 2020; Huang et al., 2016; El-Didamony et al., 2012). For example, Zhang et al. (2019) investigated the impact of SP on the flowability of cement paste. The results indicated that the inclusion of SP improved

FIGURE 1
Mechanism of superplasticizer.
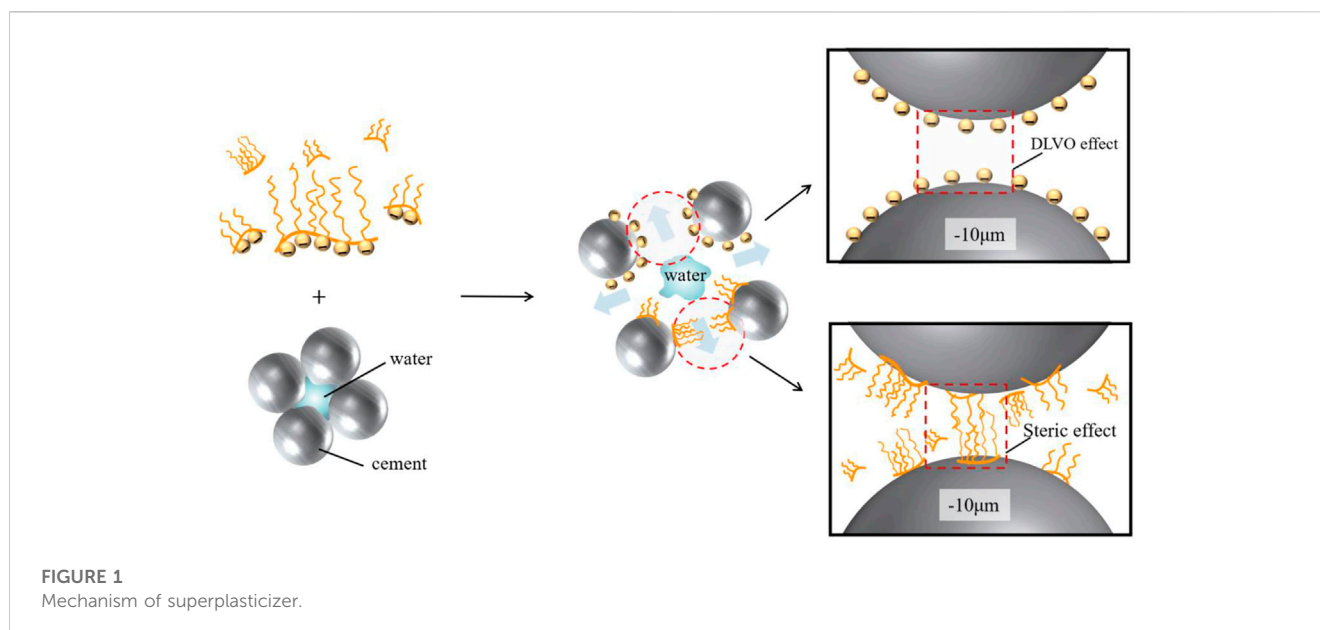
the flowability significantly (more than three times that of mixtures without SP). Similarly, Ma et al. (2020) found parallel results where the addition of appropriate SP contributes to an enhanced workability of the concrete matrix. However, the authors also concluded that the overuse of SP reduces the positive effect. With regard to the rheological properties, Zhu et al. (2021) investigated the rheological properties of concrete with SP, where the plastic viscosity and yield stress sharply reduced with increased amounts of SP. Ammar (2011) systematically investigated the rheological properties of high-performance paste mixtures, and the results indicated that a non-linear relation between the shear stress and the strain rate (variation in the viscosity of the paste mixture with the applied shear rate) could be achieved. Apart for the promotion effect on the workability and rheological properties, Zhang and Kong (2015) found a tight relationship between SP dosage and the hydration process. The authors confirmed that SP resulted in a prolonged induction period and a reduced maximum exothermic rate during the accelerated cement hydration phase. In addition, the impact of SP on the microstructure has also been surveyed. For example, He et al. (2021) found that the addition of SP contributed to more hydration products, lower porosity, and optimized the pore structure, thus leading to a denser microstructure. The impact of SP on the pore structure of concrete was investigated by Zhang et al. (Zhang and Kong, 2014), where it was discovered that the addition of SP significantly decreased the mean pore size. In addition, Zeyad and Almalki (2020) investigated the SP dosage on the mechanical properties of the concrete. The conclusions indicated that SP had a limited effect on the mechanical properties, where strengths of 33.5, 35.4, 34.3, and 33.9 MPa were obtained in specimens with 1.5%, 2%, 2.5%, and 3% SP, respectively. A similar result was achieved by Nakul et al. (2020), where an the strength inconspicuously varied from 36.4 to 40.2 MPa with an increasing amount (from 1% to 3%) of SP. Regarding the durability, Huang et al. (2016) verified that concrete with SP contributes to a comparable water penetration depth compared with that of mixtures without SP. In addition, a slight decrease (<1%) in the total chloride content further confirmed that SP had limited impact on the durability (El-Didamony et al., 2012).

The use of SP is not complicated, although multiple influences attributed to the inclusion of SP can be found. Generally, regarding the type of SP, polycarboxylate (PCE)-based SP has been commonly selected due to its greater water reduction effect as a result of both an enhanced space steric hindrance effect and a charge neutralization effect (Uchikawa et al., 1997; Gołaszewski and Szwabowski, 2004; Toledano-Prados et al., 2013). The optimized dosage can be determined mainly from the workability requirement since the impact of SP on working performance is far greater than that on other properties.

However, SP selection can be more complex in ultra-high-performance concrete (UHPC) development. As commonly acknowledged, the ultra-high compressive strength and superior durability of UHPC mainly come from particle close packing (Hou et al., 2021), and the particle packing structure can be altered by the introduction of nano-/micro-sized active or inactive materials (such as silica fume, metakaolin, and micro fly ash) (Larrard and Sedran, 1994; Li and Kwan, 2013; Wang et al., 2021a; Wang et al., 2021b; Yu et al., 2021). As a result, the accumulation of particles is crucial in UHPC systems.

It is well known that SP plays a vital role in the particle packing structure of concrete. However, different trends can be found in the strength development of conventional concrete (CC) and UHPC dominated by packing. To be specific, SP mainly influences the working performance of CC, as mentioned above. However, compared with that of CC, UHPC eliminates coarse aggregate and special high efficiency SP is applied, which greatly reduces the W/B ratio and maintains excellent fluidity. Moreover, it improves the strength of UHPC at different ages; in addition, the particle packing structure can be altered by the introduction of nano-/micro-sized active or inactive materials (such as silica fume, metakaolin, and micro fly ash) (Kwan and Ng, 2010). A compact accumulation structure is the key factor to optimize pore structure and improve the durability and strength of UHPC, while the packing structure of UHPC is easily altered because of the

TABLE 1 Chemical compositions of C, SF, and FA (wt%).

Material	CaO	SiO$_2$	Al$_2$O$_3$	Fe$_2$O$_3$	SO$_3$	K$_2$O	Na$_2$O	MgO	P$_2$O$_5$	LOI[a]
C	67.78	18.55	4.34	3.71	2.82	0.70	-	1.85	0.10	0.15
SF	0.69	95.56	0.34	0.18	1.15	0.53	0.11	0.89	0.54	0.01
FA	7.43	47.21	36.54	3.31	0.69	0.79	0.12	0.32	0.42	3.17

[a]Loss of ignition.

FIGURE 2
Chemical structure of PCE-based SP.
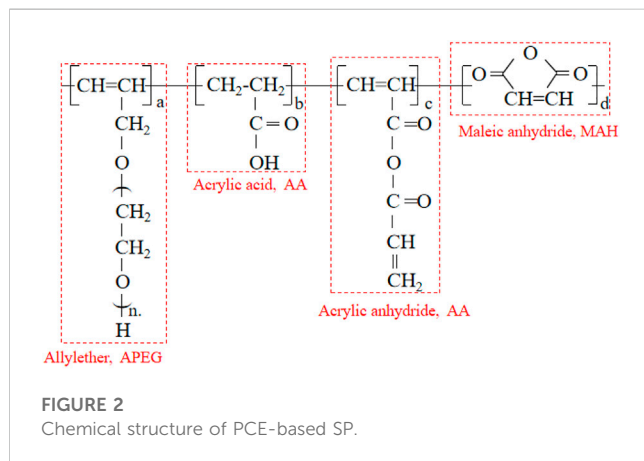
dispersion of particles, which is based on the addition of SP. In other words, the packing structure is sensitive to the amount of SP. Therefore, it is valuable to seek an optimized method of SP dosage in the UHPC. In addition, the brittleness and toughness of UHPFRC are mainly improved by the incorporation of steel fiber (Abrishambaf et al., 2013; Yoo et al., 2014; Tran et al., 2016). The fiber enhancement effect depends on the distribution and orientation of fiber and the fresh properties (mainly the plastic viscosity) of concrete, which is significantly affected by SP (Khayat et al., 2019; Wang et al., 2021c). That is to say, the settlement risk of fiber will also become sensitive to the changes of SP dosage in UHPFRC. Therefore, more attention should be paid to ensure a good distribution of fiber in UHPFRC. In summary, it can be inferred that the influence of SP on UHPC is different from that on other cementitious materials. However, SP in UHPC and UHPFRC is added in a similar method as that for ordinary concrete (according to the work performance requirement). As mentioned above, the traditional method for determining the amount of SP used will probably lead to an obvious decrease in the mechanical properties of UHPC. Thus, it is urgent to search for an effective and appropriate method for the optimization of SP in UHPC, both in view of working performance and strength development.

Based on the previous discussion, this experimental survey is undertaken to uncover the influence of SP on the performance (mainly the workability and mechanical properties) of UHPC. To achieve this, the fresh and hardened state properties of UHPC (or UHPFRC), with a constant or ultra-low W/B ratio, as a function of the SP dosage have been tested. After that, the determination of SP dosage will be provided. This study also provides ideas for the rational use of SP in UHPC and UHPFRC.

2 Materials and methods

2.1 Materials

CEM I cement (C), silica fume (SF), and fly ash (FA) were used as cementitious materials, and their chemical compositions are shown in Table 1. The specific surface areas of cement, fly ash, and silica fume are 350 m^2/kg, 352 m^2/kg, and 18381 m2/kg, respectively, and river sand with a maximum particle size of 0.6 mm was used as an aggregate. A polycarboxylic ether-based SP was chosen to investigate its impact on the properties of the UHPC matrix, and its chemical structure is shown in Figure 2. Additionally, in order to promote the strength and toughness of UHPC, steel fiber with a length of 13 mm, diameter of 0.2 mm, and tensile strength above 2200 MPa was used.

2.2 Preparation of UHPC

The modified Andreasen and Andersen (MAA) model is utilized to develop a UHPC matrix with a dense packing skeleton, using the following equation (Yu et al., 2014; Yu et al., 2015; Li et al., 2021):

$$P(D) = \frac{D^q - D_{min}^q}{D_{max}^q - D_{min}^q},\qquad(1)$$

where D is the particle size (μm), P(D) is the fraction of solids lower than size D, and Dmin and Dmax are the minimum and maximum solid size (μm), respectively. q is the distribution modulus and has been selected as 0.23 according to the overall size. After that, the matrix was developed and UHPC with an ultimate-low W/B ratio and a constant ratio of 0.23 was designed by optimizing the water content, to highlight the influence on the mechanical properties and to achieve an acceptable workability. Additionally, UHPFRC, with a steel fiber content of 2% (by volume), was prepared to investigate the interaction between SP and steel fiber. Finally, various SP dosages (ranging from 1.5% to 4.5%) were devised to evaluate the impact of SP on the performance of UHPC and UHPFRC. The mix proportions are presented in Table 2.

2.3 Experimental methodology

2.3.1 Wet packing density and water film thickness

Herein, the wet packing density rather than the dry packing density was used since it provides more accurate results (Kwan and Fung, 2009). Specifically, a mold with a 500 mL volumetric bottle

TABLE 2 Mix proportions of UHPC/UHPFRC with various W/B ratios (kg/m³).

Group	SP dosage (%)	C	SF	FA	S	SP	F	W
Constant W/B ratio without steel fiber	1.5	600	144	188	1000	14.9	-	216.3
	2.0	600	144	188	1000	19.8	-	212.3
	2.5	600	144	188	1000	24.8	-	208.3
	3.0	600	144	188	1000	29.8	-	204.3
	3.5	600	144	188	1000	34.7	-	200.4
	4.0	600	144	188	1000	39.7	-	196.4
	4.5	600	144	188	1000	44.6	-	192.5
Ultimate-low W/B ratio without steel fiber	1.5	600	144	188	1000	14.9	-	196.4
	2.0	600	144	188	1000	19.8	-	182.5
	2.5	600	144	188	1000	24.8	-	168.6
	3.0	600	144	188	1000	29.8	-	164.7
	3.5	600	144	188	1000	34.7	-	160.7
	4.0	600	144	188	1000	39.7	-	147.4
	4.5	600	144	188	1000	44.6	-	142.9
Constant W/B ratio with steel fiber	1.5	600	144	188	1000	14.9	156	216.3
	2.0	600	144	188	1000	19.8	156	212.3
	2.5	600	144	188	1000	24.8	156	208.3
	3.0	600	144	188	1000	29.8	156	204.3
	3.5	600	144	188	1000	34.7	156	200.4
	4.0	600	144	188	1000	39.7	156	196.4
	4.5	600	144	188	1000	44.6	156	192.5
Ultimate-low W/B ratio with steel fiber	1.5	600	144	188	1000	14.9	156	201.4
	2.0	600	144	188	1000	19.8	156	187.5
	2.5	600	144	188	1000	24.8	156	173.6
	3.0	600	144	188	1000	29.8	156	169.7
	3.5	600	144	188	1000	34.7	156	165.7
	4.0	600	144	188	1000	39.7	156	152.4
	4.5	600	144	188	1000	44.6	156	147.9

C, cement; SF, silica fume; FA, fly ash; S, sand; SP, superplasticizer; F, steel fiber; W, water.

and 150 ± 5 mm bottom side diameter (shown in Figure 3) was used, and the wet packing density was calculated using Eqs. 2, 3 (the solid volume of the cementitious materials, maximum mass, and volume of the paste in the mold are defined as V_b, M_{max}, and V, respectively):

$$\phi_{max} = \frac{V_b}{V}, \qquad (2)$$

$$V_b = \frac{M_{max}}{R_C \rho_C + R_S \rho_S + R_f \rho_f + V_w \rho_w}, \qquad (3)$$

in which ρ_w is the density of water (kg/m³); V_w is the volumetric water–binder ratio; ρ_c, ρ_s, and ρ_f are the solid densities of the cement, silica fume, and fly ash (kg/m³), respectively; and R_c, R_s, and R_f are the volumetric ratios of the cement, silica fume, and fly ash to the total cementitious materials, respectively.

Based on the water film theory proposed by Kwan (Kwan et al., 2010), when water is filled into the space of the cementitious material particles, any remaining water is wrapped on the surface of the cementitious material to form a water film with uniform thickness; the formula for calculating the water film thickness (WFT) (μm) of cementitious particles is as follows:

$$WFT = \frac{V_{ew}}{A}, \qquad (4)$$

$$V_{ew} = V_w - V_v, \qquad (5)$$

$$V_v = \left(\frac{1}{\varphi_{max}} - 1\right)\left(\frac{M_c}{\rho_c} + \frac{M_f}{\rho_f} + \frac{M_s}{\rho_s}\right), \qquad (6)$$

$$A = M_c A_c + M_f A_f + M_s A_s, \qquad (7)$$
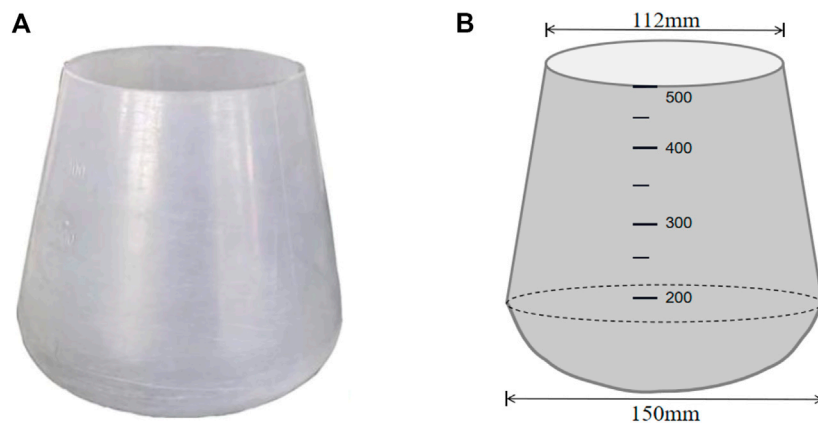
FIGURE 3
Digital image **(A)** and diagram photo **(B)** of the equipment used for the wet packing density.

FIGURE 4
Schematic diagram of the **(A)** slump flow equipment and **(B)** mini V-funnel.

where V_{ew} is the volume of the remaining water; A is the total surface area of the cementitious material (m^2); V_w is the actual volume of water for the sample (m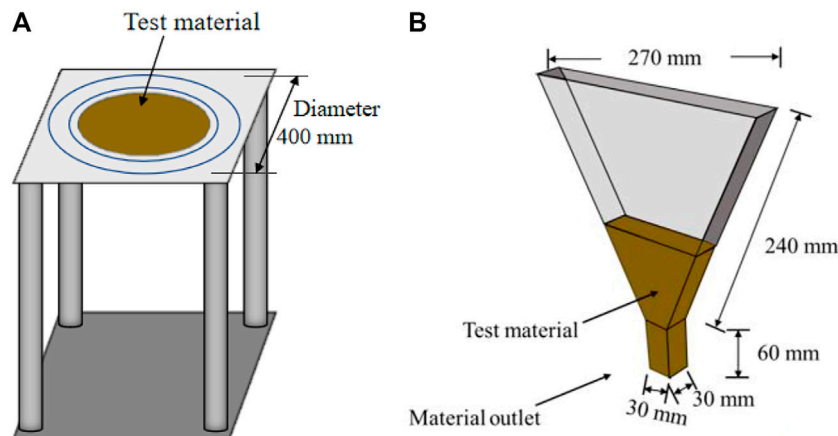L); V_v is the volume of the inter particle space (mL); ρ_c, ρ_s, and ρ_f represent the solid densities of the cement, silica fume, and fly ash (kg/m^3), respectively; M_c, M_s, and M_f are the masses of cement, silica fume, and fly ash used in the sample (g); and A_c, A_f, and A_s are the specific surface areas of cement, silica fume, and fly ash (m^2/kg), respectively.

2.3.2 Workability

A 400 mm diameter test stand is used (without any vibration) to measure the slump flow according to EN 1015-3 (EN 1015-3, 1999). The mini V-funnel test refers to the EFNARC method (EFNARC, 2002), which is used to test the flow time. A schematic diagram of the equipment used is presented in Figure 4.

2.3.3 Setting time

The initial setting time of the slurry was measured using a Vicat needle according to EN 196-3 (BS EN 196-3, 2017).

2.3.4 Mechanical properties

The compressive strength was tested according to EN 196-1 (EN 196-1 Chapter13, 2016).

2.3.5 Fiber distribution evaluation

Yoo et al. (2016) explored the fiber distribution of UHPERC based on sample sectional images (Lee et al., 2009). Hence, the concrete specimens were cut using a steel blade, and sectional images were acquired with high-resolution equipment. After that, binary images were obtained using binary processing software. Finally, the formula of the fiber distribution coefficient α_f is
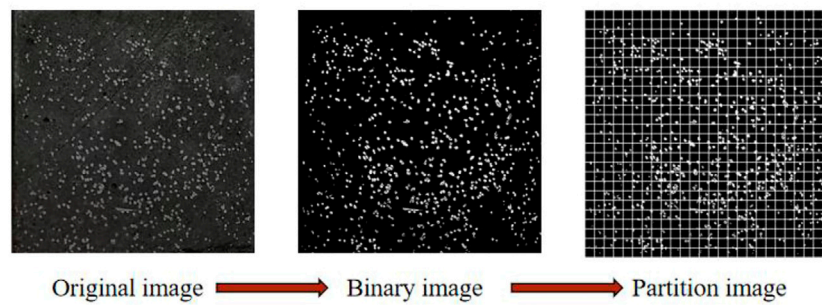
FIGURE 5
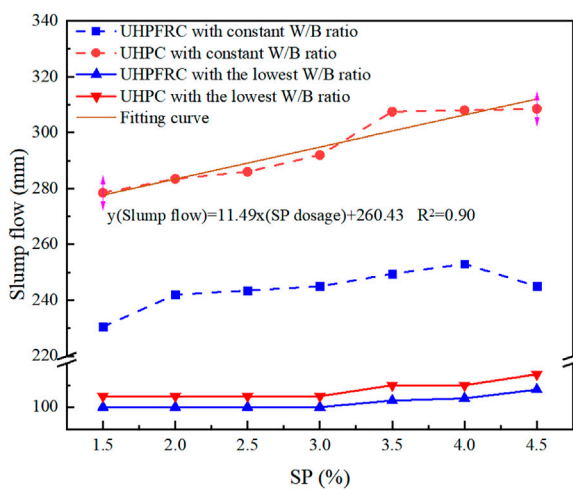Original, binary, and partition images of UHPFRC.

FIGURE 6
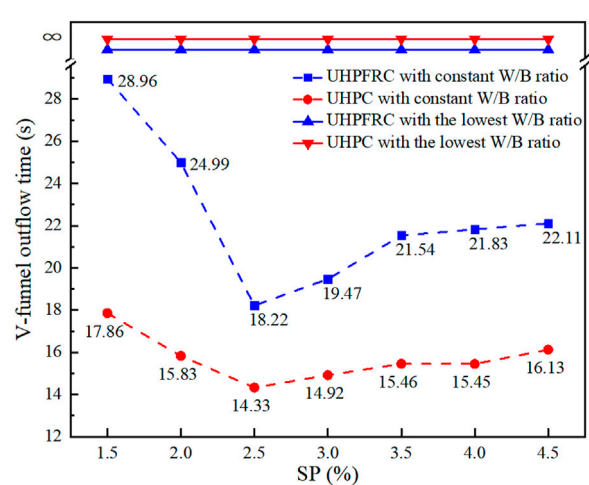Influence of SP dosage on the slump flow of UHPC and UHPFRC with various W/B ratios.

FIGURE 7
Influence of SP dosage on the mini V-funnel outflow time of UHPC and UHPFRC with various W/B ratios.

$$\alpha_f = \exp\left[-\sqrt{\frac{\sum (x_i - 1)^2}{n}}\right], \quad (8)$$

where n is the total fiber number in the sectional image and x_i is the fiber number in the i_{th} unit (the image is split into n units, and it is assumed that a fiber occupies a unit when the fibers are completely uniformly distributed). Original, binary, and partition images are shown in Figure 5.

3 Results and discussion

3.1 Slump flow

Figure 6 illustrates the slump flow of UHPC (with fiber reinforcement or without) versus various SP dosages. It can be observed that all specimens with a constant W/B ratio of 0.23 show significantly enhanced workability compared to the paste with the ultimate-low W/B ratio due to the increased amount of free water.

Specifically, the slump flow of specimens with constant W/B ratio falls in the range of 220–260 mm, while a sharply reduced slump flow (with maximum value of 110 mm) can be witnessed in groups with the ultimate-low W/B ratio. Regarding the UHPC and UHPFRC with relatively lower W/B ratio, slump flows of approximately 100 mm indicate that the "dry" mixtures almost lose their fluidity. Additionally, it can be noticed that the introduction of steel fiber further alters the workability. For example, a maximum decrease of 21% can be witnessed in specimens with constant W/B ratio, while a slight alteration can be observed due to the poor fluidity in specimens with a much lower W/B ratio (0.14–0.16).

In addition, the inclusion of SP has various impacts. For UHPC and UHPFRC with constant W/B ratio, the workability gradually improved with the increase of SP up to 3.5%. Specifically, the slump flow of the control group is 271 mm, while it linearly increases to 278.5 mm, 286.0 mm, 307.5 mm in mixtures with 1.5%, 2.5%, and 3.5% SP, respectively. The obtained experimental results in this study are in line with those shown in the previous literature (Li et al., 2017), where the water locked in the flocculation structure can be released due to the space steric hindrance effect and charge neutralization effect attributed to the SP. However, it should be

FIGURE 8
Influence of the dosage of SP on the WFT and wet packing density of UHPC.
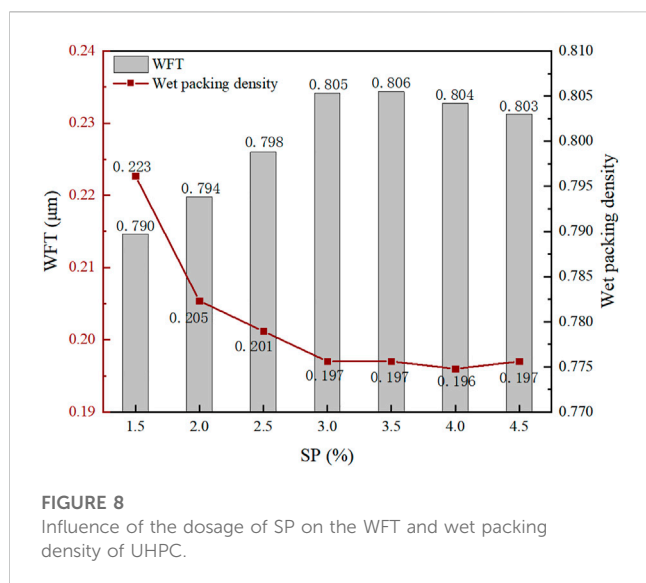
noted that further inclusion of SP reduces the enhancement effect, where an almost unchanged slump flow of 308.0 mm and 308.5 mm are witnessed in specimens with 4.0% and 4.5% SP, respectively.

3.2 Mini V-funnel time

Due to its high powder content and ultra-low W/B ratio, UHPC suffers a much higher viscosity compared with that of conventional concrete although UHPC contributes to a large slump flow. Therefore, except for the static evaluation approach of workability, a dynamic testing method for characterizing the workability, i.e., the mini V-funnel outflow time has been used to investigate the working performance of UHPC and UHPFRC paste. The results are illustrated in Figure 7. It can be found that UHPC failed to pass the funnel since it has poor workability, while flow times ranging from 18.22 s to 28.96 s (or 14.33 s–28.96 s) can be generated depending on the introduction of steel fiber (or not) in the group with the constant W/B ratio. Specifically, a V-shaped line trend (decreases first and then increases with the increase of SP) can be witnessed, and the lowest outflow time of 14.33 s is obtained in specimens with 2.5% SP. The reason for this can be clarified as follows: on the one hand, the inclusion of SP releases free water and improves the workability as aforementioned, and on the other hand, the introduction of SP increases the viscosity, which reduces the passing ability of the slurry. For UHPC with less SP, the enhancement in workability dominates, while in specimens with a large dosage of SP, the negative effects of viscosity dominate.

3.3 Water film thickness and wet packing density

The WFT and wet packing density are tested merely based on plain concrete (there is no suitable method to evaluate the packing density of UHPFRC at present due to the fiber network). The WFT and wet packing density of UHPC slurry versus various dosages of SP are illustrated in Figure 8. It can be

clearly seen that the WFT shows a continuous decreasing trend from 0.233 µm to 0.197 µm in mixtures with up to 3.5% SP, and this lower value is maintained with the further increase of SP dosage. For the wet packing density, an opposite trend is generated, where the maximum wet packing density can be seen in specimens with 3.5% SP. The opposite trends of the variation of wet packing density and WFT can be explained as follows: SP alters the electrical properties of the cement particle by coating the particle surface, making the cement produce electrostatic repulsion, thus dispersing the cement particles, releasing the water locked by cement aggregation (as discussed in Section 3.1), decreasing the average WFT, and increasing the packing density; a schematic diagram of the packing structure is shown in Figures 9A, B. However, it is noteworthy that further addition of SP decreases the packing density although a constant WFT value is maintained. The reason for this is attributed to the increased amount of air bubbles caused by the further introduction of SP (as shown in Figure 9C). These results are consistent with the study by Yu et al. (2021), where the alteration of wet packing density also follows a parabolic law.

3.4 Setting time

The initial setting time of UHPC in the state of constant W/B ratio and minimum W/B ratio versus the SP dosage is illustrated in Figure 10. It can be clearly observed that specimens with a constant W/B ratio suffer a relatively longer setting time compared with that of UHPC with the lowest W/B ratio. For example, an average time of 15 min is observed for mixtures with 2.0%, 2.5%, 3.0%, and 3.5% SP. It can be noticed that the setting time of UHPC with the lowest W/B ratio has a similar tendency, except for specimens with 2.0% SP content. This phenomenon is mainly due to the fact that the lower W/B ratio results in more closely packed particles, where the particles can be connected with less hydration products, thus forming into a solid-connected structure. Furthermore, the retarding effect caused by SP has been well studied, where 1) the introduction of SP reduced the WFT (discussed in Section 3.2), prevented the cement particles from reacting with water, hindered the hydration process of cement, and thus, increased the setting time (Li et al., 2014). 2) The $-COO^-$ group formed a complex compound with Ca^{2+} produced during cement hydration, which reduced the concentration of Ca^{2+}, delayed the formation of the hydrated product $Ca(OH)_2$, and consequently, prolonged the setting time (Chen et al., 2021; Zhu et al., 2022).

3.5 Compressive strength

The 28-day mechanical properties of UHPC and UHPFRC with different SP dosages are illustrated in Figure 11. For UHPC without fiber reinforcement, it can be clearly seen that the group with a constant W/B ratio (0.23) suffers a relatively lower strength development compared with that of the group with an ultimate-low W/B ratio (ranging from 103.7 to 137.7 MPa depending on the dosage of SP). There is no doubt that a lower W/B ratio benefits strength development, which has been proved
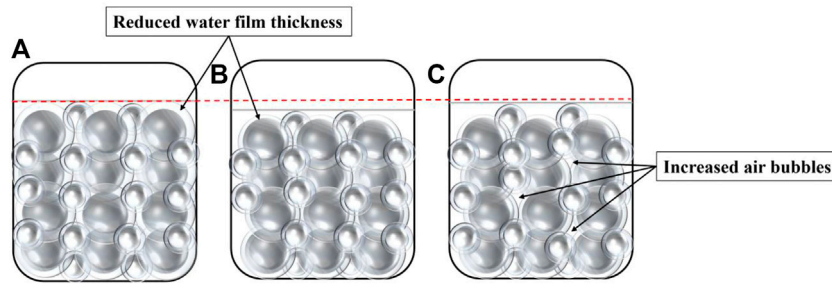
FIGURE 9
Particle packing structure **(A)** without SP, **(B)** with the inclusion of SP, and **(C)** with the overuse of SP.
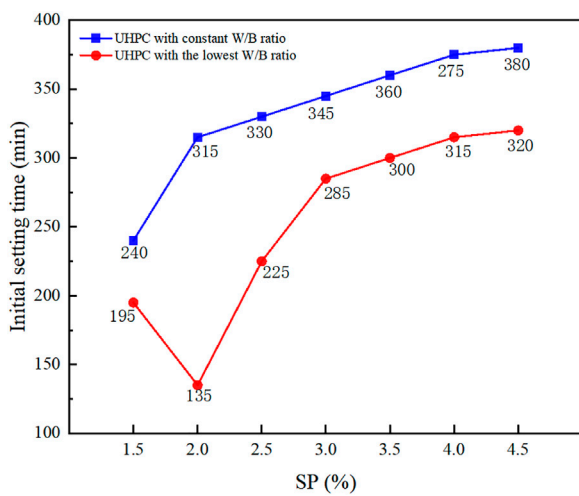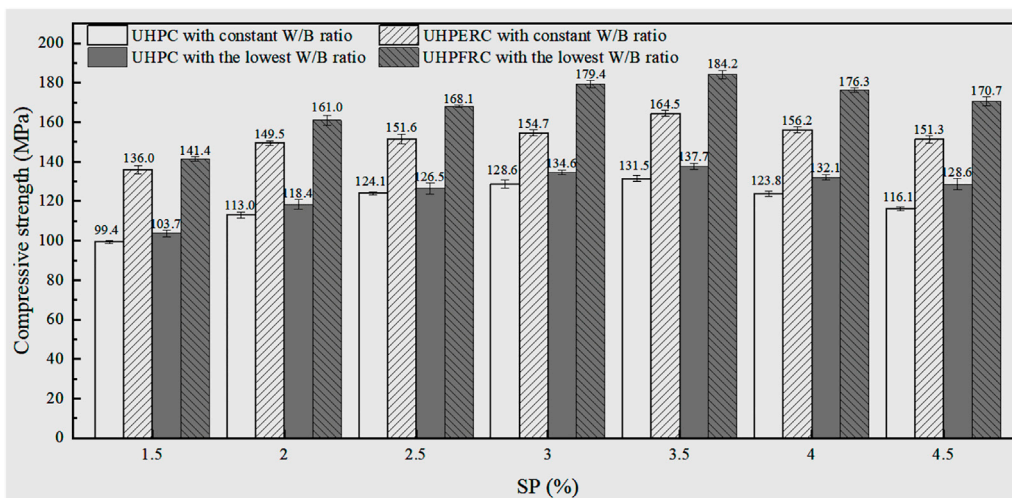

FIGURE 10
Influence of SP dosage on the slump flow of UHPC and UHPFRC with various W/B ratios.

by numerous studies. Among them, the most well-known presents the Bolomey formula, as shown in Eq. 9, which explains the relationship between the W/B ratio and strength development:

$$\frac{W}{B} = \frac{\alpha_a f_{ce}}{f_{cu,0} + \alpha_a \alpha_b f_{ce}}, \quad (9)$$

where α_a and α_b are two regression constants related to aggregates, f_{ce} is the 28-day compressive strength of composite cement mortar, and $f_{cu,0}$ is the compressive strength. It can be seen that the variation of SP has limited effects on the compressive strength of specimens with a constant W/B ratio, with a strength variation range within 6% when the SP content is 2.5%–4.5%. In contrast, for specimens with a constant W/B value, a parabolic trend can be witnessed for UHPC with a ultimate-low W/B ratio, and the optimal SP dosage considering compressive strength enhancement is 3.5%. A maximum strength of 182.2 MPa can be obtained, beyond which further addition of SP would degrade the mechanical properties of UHPC.

Excitingly, we obtained a proportional relationship when comparing the 28-day compressive strength and wet packing density (Section 3.3) against the SP dosage. Specifically, a

FIGURE 11
Influence of SP dosage on the compressive strength of UHPC (UHPFRC).

FIGURE 12
Enhanced efficiency of the steel fiber in specimens with various W/B ratios.

products are directly determined by the accumulation, further affecting the strength development of concrete.

The strength enhancement efficiency of UHPFRC with the various SP contents is shown in Figure 12. For UHPC containing fiber, an obvious strength increase is observed. For instance, a 34% increase in the average strength is seen upon fiber addition to UHPC with the lowest W/B ratio. Nevertheless, the situation is more complex in specimens with a constant W/B ratio, where SP dosages of 2.5% and 3% only produced an approximately 20% increase, which is half of that of the other groups (the strength of the 1.5% SP group increased by 39%). The reason for this lies in the changes in fiber distribution, which are determined by the working performance of the concrete paste. Generally, steel fibers, with the advantages of being small and stable, are interwoven inside the slurry to form a fiber network, and, the more freely the fibers are distributed, the higher the generated strength; otherwise, the strength will be diminished. Thus, mixtures with fiber settlement (SP content of 2.5% and 3%) contribute to a much lower reinforcement and exhibit degraded mechanical properties (which will be discussed in Section 3.6).

3.6 Fiber-reinforced efficiency

Binary images illustrating the effect of SP on the fiber distribution coefficient in specimens with the constant W/B ratio are presented in Figure 13. It is observed that the fiber settlement behavior becomes increasingly clear in specimens with 2.0% and 2.5% SP. For a more accurate evaluation of the distribution coefficient which has been calculated using Eq. 8 to quantify the impact, the fiber distribution coefficient of UHPFRC with the constant W/B ratio is plotted in Figure 14. Generally, the distribution coefficient is close to 1 when the fiber distribution is uniform, and a coefficient larger than 0.3 indicates a well-distributed fiber distribution (BS EN 196-3, 2017). From the calculation results, we can observe that the fiber distribution
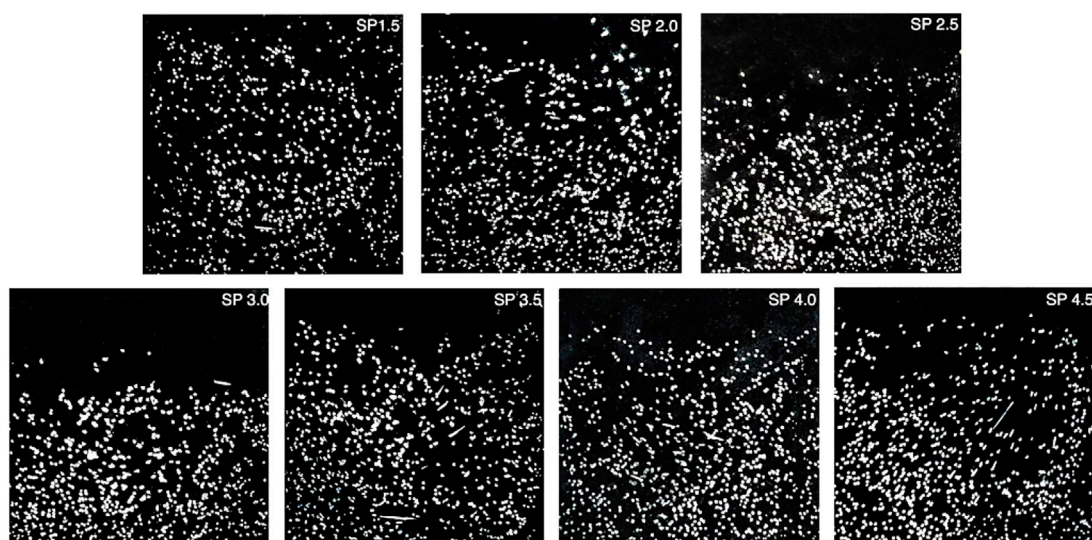
maximum strength of 182.2 MPa and a maximum packing density of 0.806 can be found for SP 3.5%. Packing plays an important role in determining the strength development. However, with an emphasis on packing, the reduction of the W/B ratio contributes to improved packing density, except for the widely recognized fact that accumulation is able to reduce the space between the particles. Moreover, the decreased amount of liquid phase also leads to dense accumulation, which alters the initial state of hydration because of the presence of ultra-fine particles that have pozzolanic activity. These generate a more compact structure in concrete due to their participation in the hydration of cement, forming C-S-H. The properties of hydration

FIGURE 13
Binary images of the UHPC with different dosages of SP.

FIGURE 14
Fiber distribution coefficient of UHPFRC with the constant W/B ratio.
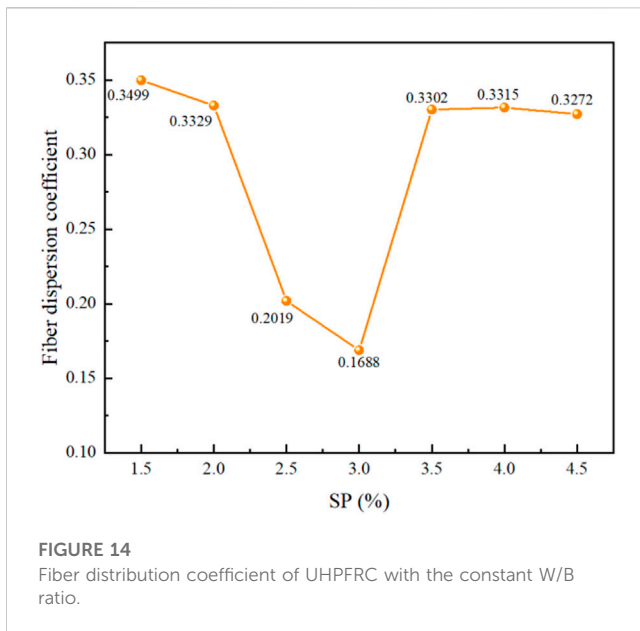
coefficients of UHPFRC with different SP dosages range from 0.1688 to 0.3499. Thus, the relatively lower coefficients of 0.2019 and 0.1688 further confirmed that UHPFRC with 2.5% and 3.0% SP suffer high risks of fiber distribution. It is well known that fiber settlement is dominated by the rheological properties, especially the viscosity of concrete. With the inclusion of SP, the water in the flocculation structure of the cement can be released, thus reducing the viscosity. As a result, degraded fiber distribution occurs, where the trend is in line with the V-funnel flow time shown in Section 3.1. However, it is worth noting that the risk of fiber settlement decreases with the further addition of SP, where increased fiber distribution coefficients of 0.3302, 0.3315, and 0.3272 can be witnessed. This phenomenon is attributed to the increased viscosity caused by the inclusion of SP as mentioned above.

4 Conclusion

In this article, the impacts of SP on the performance of UHPC and UHPFRC have been revealed. The main conclusions are as follows:

(1) For UHPC with a constant W/B ratio, the addition of SP mainly affects the fresh behavior. Specifically, the slump flow of the UHPC increased and the V-funnel time shortened obviously with the addition of less than 3% SP. The further addition of SP contributes to a less positive effect on the workability. Moreover, an obvious increase in the setting time can be witnessed *via* the inclusion of SP.

(2) For UHPFRC with the constant W/B ratio, SP has a significant impact on both the workability and compressive strength development. Regarding the workability, the addition of SP generates a similar trend compared with that in UHPC with a constant W/B ratio, except for a reduced workability due to the formation of a fiber network structure. In addition, it is noteworthy that the enhancement efficiency of the fiber significantly reduced the risk of fiber settlement, thus affecting the strength development. The SP content should be 3.5%, based on the high-fiber reinforcement effect under the premise of suitable working performance conditions.

(3) For the UHPC and UHPFRC with the lowest ratio, SP determines the strength development of UHPC (UHPFRC) by impacting the packing system. Specifically, the inclusion of SP reduces the WFT, thus optimizing the pore structure and the particle packing structure. As a result, enhanced mechanical properties can be obtained. However, the overuse of SP impedes superior performance and weakens the enhancement effect due to the air-entraining action. For the lowest W/B ratio system (with or without steel fiber), the optimal amount of SP is 3.5%.

In conclusion, by studying four systems, it is proved that SP plays a different role in UHPC than in CC and high-performance concrete (HPC). The most obvious difference is that the SP directly affects the mechanical properties of UHPC (influencing the strength of UHPFRC by indirect means and directly by the particle packing density). Therefore, in the selection of SP more attention should be paid to its impact on strength development rather than work performance. Based on the aforementioned results, the optimum dosage of SP considering the work performance is 3.0%, and 3.5% is selected where the mechanical properties are more important. This study still has some limitations, and further research is needed. For example, the SP was not synthesized by ourselves and the choice was unitary; therefore, the evaluation of durability and dimensional stability is not completely comprehensive.

Data availability statement

The original contributions presented in the study are included in the article/Supplementary Material; further inquiries can be directed to the corresponding author.

Author contributions

LW: conceptualization, methodology, and software; YM: data curation and writing—original draft preparation; and LL: data curation and software.

Funding

Conflict of interest

The authors declare that the research was conducted in the absence of any commercial or financial relationships that could be construed as a potential conflict of interest.

Publisher's note

All claims expressed in this article are solely those of the authors and do not necessarily represent those of their affiliated organizations, or those of the publisher, the editors, and the reviewers. Any product that may be evaluated in this article, or claim that may be made by its manufacturer, is not guaranteed or endorsed by the publisher.

References

Abrishambaf, A., Barros, J. A. O., and Cunha, V. M. C. F. (2013). Relation between fibre distribution and post-cracking behaviour in steel fibre reinforced self-compacting concrete panels. *Concr. Res.* 51, 57–66. doi:10.1016/j.cemconres.2013.04.009

Ammar, Y. (2011). Shear-thickening behavior of high-performance cement grouts - influencing mix-design parameters. *Cem. Concr. Res.* 41 (3), 230–235. doi:10.1016/j.cemconres.2010.11.004

Boscaro, F., Palacios, M., and Flatt, R. J. (2021). Formulation of low clinker blended cements and concrete with enhanced fresh and hardened properties. *Cem. Concr. Res.* 150, 106605. doi:10.1016/j.cemconres.2021.106605

Bs En 196-3 Methods of testing cement - Part 3: Determination of setting times and soundness, 2017, https://standards.iteh.ai/catalog/standards/cen/e4921eca-8101-4261-b066-25d19b9b8e8a/en-196-3-2016.

Chen, S. L., Zhang, J. L., Sun, S. M., Zhong, K., Shao, Q., Xu, H., et al. (2021). Dispersion, fluidity retention and retardation effect of polyacrylate-based ether superplasticizer nanomicelles in Portland cement. *Constr. Build. Mater.* 290, 123149. doi:10.1016/j.conbuildmat.2021.123149

Efnarc (2002). Specification and guidelines for self-compacting concrete. *Rep. EFNARC.* 44, 32.

El-Didamony, H., Mohamed, H., Khalil, K., and Al-Masry, S. (2012). Effect of delaying addition time of SMF superplasticizer on the physico-mechanical properties and durability of cement pastes. *Constr. Build. Mater.*, 35, 261–269. doi:10.1016/j.conbuildmat.2012.02.068

En 1015-3 (1999). *Methods of test for mortar for masonry, Part 3 determ. Consistence fresh mortar.* https://standards.iteh.ai/catalog/standards/cen/f427f20a-2746-4ab7-bd55-d1c455b1f009/en-1015-3-1999, (by Flow Table).

En 196-1 Chapter13 (2016). Cement - determination of strength. *Build. Mater. 10 - Test. Methods.*, 66–71.

Gołaszewski, J., and Szwabowski, J. (2004). Influence of superplasticizers on rheological behaviour of fresh cement mortars. *Cem. Concr. Res.* 34 (2), 235–248. doi:10.1016/j.cemconres.2003.07.002

He, Y., Liu, S. H., Luo, Q., Liu, W., and Xu, M. (2021). Influence of PCE-type GA on cement hydration performances. *Constr. Build. Mater.* 302, 124432. doi:10.1016/j.conbuildmat.2021.124432

Hou, D. S., Wu, D., Wang, X. P., Gao, S., Yu, R., Li, M. M., et al. (2021). Sustainable use of red mud in ultra-high performance concrete (UHPC): Design and performance evaluation. *Cem. Concr. Comp.* 115, 103862. doi:10.1016/j.cemconcomp.2020.103862

Huang, H. L., Qian, C. X., Zhao, F., Qu, J., Guo, J., and Danzinger, M. (2016). Improvement on microstructure of concrete by polycarboxylate superplasticizer (PCE) and its influence on durability of concrete. *Constr. Build. Mater.* 110, 293–299. doi:10.1016/j.conbuildmat.2016.02.041

Khayat, K. H., Meng, W., Vallurupalli, K., and Teng, L. (2019). Rheological properties of ultra high performance concrete-An overview. *Cem. Concr. Res.* 124, 105828. doi:10.1016/j.cemconres.2019.105828

Kwan, A. K. H., and Fung, W. W. S. (2009). Packing density measurement and modelling of fine aggregate and mortar. *Cem. Concr. Compos.* 31 (6), 349–357. doi:10.1016/j.cemconcomp.2009.03.006

Kwan, A. K. H., Fung, W. W. S., and Wong, H. H. C. (2010). Water film thickness, flowability and rheology of cement-sand mortar. *Adv. Cem. Res.* 22 (1), 3–14. doi:10.1680/adcr.2008.22.1.3

Kwan, A. K. H., and Ng, I. Y. T. (2010). Improving performance and robustness of SCC by adding supplementary cementitious materials. *Constr. Build. Mater.* 24 (11), 2260–2266. doi:10.1016/j.conbuildmat.2010.04.030

Lange, A., Hirata, T., and Plank, J. (2014). Influence of the HLB value of polycarboxylate superplasticizers on the flow behavior of mortar and concrete. *Cem. Concr. Res.* 60, 45–50. doi:10.1016/j.cemconres.2014.02.011

Larrard, F. D., and Sedran, T. (1994). Optimization of ultra-high-performance concrete by the use of a packing model. *Cem. Concr. Res.* 24 (6), 997–1009. doi:10.1016/0008-8846(94)90022-1

Lee, B. Y., Kim, J. K., Kim, J. S., and Kim, Y. Y. (2009). Quantitative evaluation technique of polyvinyl alcohol (PVA) fiber dispersion in engineered cementitious composites. *Cem. Concr. Compos.* 31 (6), 408–417. doi:10.1016/j.cemconcomp.2009.04.002

Li, J. H., Wang, X. P., Chen, D. D., Wu, D., Han, Z., Hou, D., et al. (2021). Design and application of UHPC with high abrasion resistance. *Constr. Build. Mater.* 309, 125141. doi:10.1016/j.conbuildmat.2021.125141

Li, L. G., and Kwan, A. K. H. (2013). Concrete mix design based on water film thickness and paste film thickness. *Cem. Concr. Compos.* 39, 33–42. doi:10.1016/j.cemconcomp.2013.03.021

Li, P. P., Yu, Q. L., and Brouwers, H. J. H. (2017). Effect of PCE-type superplasticizer on early-age behaviour of ultra-high performance concrete (UHPC). *Constr. Build. Mater.* 153, 740–750. doi:10.1016/j.conbuildmat.2017.07.145

Li, Y. W., Yang, C. L., Zhang, Y. F., Zheng, J., Guo, H., and Lu, M. (2014). Study on dispersion, adsorption and flow retaining behaviors of cement mortars with TPEG-type polyether kind polycarboxylate superplasticizers. *Constr. Build. Mater.* 64, 324–332. doi:10.1016/j.conbuildmat.2014.04.050

Ma, B. G., Qi, H. H., Tan, H. B., Su, Y., Li, X., Liu, X., et al. (2020). Effect of aliphatic-based superplasticizer on rheological performance of cement paste plasticized by polycarboxylate superplasticizer. *Constr. Build. Mater.* 233, 117181. doi:10.1016/j.conbuildmat.2019.117181

Nakul, G., Ankur, G., and Kuldeep, K. (2020). Mechanical and durability properties of geopolymer concrete composite at varying superplasticizer dosage. *Mater. Today: Proc.* 44, 12–16.

Othmane, B., El-Hadj, K., and Said, K. (2012). Effects of granulated blast furnace slag and superplasticizer type on the fresh properties and compressive strength of self-compacting concrete. *Cem. Concr. Comp.* 34 (4), 583–590. doi:10.1016/j.cemconcomp.2011.08.013

Toledano-Prados, M., Lorenzo-Pesqueira, M., González-Fonteboa, B., and Seara-Paz, S. (2013). Effect of polycarboxylate superplasticizers on large amounts of fly ash cements. *Build. Mater.* 48, 628–635. doi:10.1016/j.conbuildmat.2013.07.069

Tran, N. T., Kiet Tran, T., Jeon, J. K. y., Park, J. K., and Kim, D. J. (2016). Fracture energy of ultra high performance fiber reinforced concrete at high strain rates. *Cem. Concr. Res.* 79, 169–184. doi:10.1016/j.cemconres.2015.09.011

Uchikawa, H., Hanehara, S., and Sawaki, D. (1997). The role of steric repulsive force in the dispersion of cement particles in fresh paste prepared with organic admixture. *Cem. Concr. Res.* 27 (1), 37–50. doi:10.1016/s0008-8846(96)00207-4

Wang, L., He, T. S., Zhou, Y. X., Tang, S., Tan, J., Liu, Z., et al. (2021). The influence of fiber type and length on the cracking resistance, durability and pore structure of face slab concrete. *Constr. Build. Mater.* 2021 (282), 122706. doi:10.1016/j.conbuildmat.2021.122706

Wang, L., Jin, M. M., Guo, F. X., Wang, Y., and Tang, S. (2021). Pore structural and fractal analysis of the influence of fly ash and silica fume on the mechanical property and abrasion resistance of concrete. *Fractals* 29 (02), 2140003. doi:10.1142/s0218348x2140003x

Wang, X. P., Wu, D., Zhang, J. R., Yu, R., Hou, D., and Shui, Z. (2021). Design of sustainable ultra-high performance concrete: A review. *Constr. Build. Mater.* 307, 124643. doi:10.1016/j.conbuildmat.2021.124643

Yoo, D.-Y., Kang, S.-T., and Yoon, Y.-S. (2014). Effect of fiber length and placement method on flexural behavior, tension-softening curve, and fiber distribution characteristics of UHPFRC. *Constr. Build. Mater.* 64, 67–81. doi:10.1016/j.conbuildmat.2014.04.007

Yoo, D. Y., Banthia, N., Kang, S. T., and Yoon, Y. S. (2016). Effect of fiber orientation on the rate dependent flexural behavior of ultra-high-performance fiber-reinforced concrete. *Compos. Struct.* 157, 62–70. doi:10.1016/j.compstruct.2016.08.023

Yu, R., Spiesz, P., and Brouwers, H. J. H. (2015). Development of an eco-friendly Ultra-High Performance Concrete (UHPC) with efficient cement and mineral admixtures uses. *Cem. Concr. Comp.* 55, 383–394. doi:10.1016/j.cemconcomp.2014.09.024

Yu, R., Spiesz, P., and Brouwers, H. J. H. (2014). Mix design and properties assessment of ultra-high performance fibre reinforced concrete (UHPFRC). *Cem. Concr. Res.* 56, 29–39. doi:10.1016/j.cemconres.2013.11.002

Yu, R., Zhou, F. J., Yin, T. Y., Wang, Z., Ding, M., Liu, Z., et al. (2021). Uncovering the approach to develop ultra-high performance concrete (UHPC) with dense meso-structure based on rheological point of view: Experiments and modeling. *Constr. Build. Mater.* 271, 121500. doi:10.1016/j.conbuildmat.2020.121500

Zeyad, A. M., and Almalki, A. (2020). Influence of mixing time and superplasticizer dosage on self-consolidating concrete properties. *J. Mater. Res. Technol.* 9 (3), 6101–6115. doi:10.1016/j.jmrt.2020.04.013

Zhang, K., Pan, L. S., Li, J. H., Lin, C., Cao, Y., Xu, N., et al. (2019). How does adsorption behavior of polycarboxylate superplasticizer effect rheology and flowability of cement paste with polypropylene fiber. *Cem. Concr. Comp.* 95, 228–236. doi:10.1016/j.cemconcomp.2018.11.003

Zhang, Y., and Kong, X. (2014). Influences of superplasticizer, polymer latexes and asphalt emulsions on the pore structure and impermeability of hardened cementitious materials. *Constr. Build. Mater.* 53, 392–402. doi:10.1016/j.conbuildmat.2013.11.104

Zhang, Y. R., and Kong, X. M. (2015). Correlations of the dispersing capability of NSF and PCE types of superplasticizer and their impacts on cement hydration with the adsorption in fresh cement pastes. *Cem. Concr. Res.* 69, 1–9. doi:10.1016/j.cemconres.2014.11.009

Zhu, J. F., Hui, J., Luo, H. J., Zhang, B., Wei, X., Wang, F., et al. (2021). Effects of polycarboxylate superplasticizer on rheological properties and early hydration of natural hydraulic lime. *Cem. Concr. Comp.* 122, 104052. doi:10.1016/j.cemconcomp.2021.104052

Zhu, W. W., Feng, Q. G., Luo, Q., Yan, J., and Lu, C. (2022). Investigating the effect of polycarboxylate-ether based superplasticizer on the microstructure of cement paste during the setting process. *Case Stud. Constr. Mater.* 16, e00999. doi:10.1016/j.cscm.2022.e00999